https://doi.org/10.5194/egusphere-2023-2322
Preprint. Discussion started: 17 October 2023

A storm-relative climatology of compound hazards in Mediterranean cyclones

Raphaël Rousseau-Rizzi[1], Shira Raveh-Rubin[2], Jennifer Catto[3], Alice Portal[1], Yonatan Givon[2], and Olivia Martius[1]

[1]Institute of Geography, University of Bern, Hallerstrasse 12, CH-3012 Bern, Switzerland
[2]Department of Earth and Planetary Sciences, Weizmann Institute of Science, Rehovot 7610001, Israel
[3]College of Engineering, Mathematics and Physical Sciences, University of Exeter, Harrison Building, Streatham Campus, N Park Rd, Exeter, EX4 4QF, UK

Correspondence: Raphaël Rousseau-Rizzi (r.rousseaurizzi@gmail.com)

https://doi.org/10.5194/egusphere-2023-2322
Preprint. Discussion started: 17 October 2023

Abstract. Cyclones are responsible for much of the weather damage in the Mediterranean region, and while their association with individual weather hazards is well understood, their association with impactful multivariate compound hazards remains to be quantified. This study aims to establish a storm-relative climatology of three different multivariate hazards in Mediterranean cyclones. Namely, the co-occurrences of rain and wind, rain and wave, and particulate matter and heat are composited relative to storm centers. Composites are computed for various large-scale environments using a recent cyclone classification, which shows that few different large scale configurations lead to each compound event type. Compound rain and wind events are mostly associated with frontal cyclones and cyclones induced by anticyclonic Rossby wave breaking from late fall to early spring in the northern Mediterranean. Compound rain and wave events occur at similar times and locations, but are also associated with cyclonic Rossby wave breaking. Particulate matter and heat compound events are associated with heat lows, daughter cyclones and anticyclonic Rossby wave breaking in the warm season and over North-Africa. Next, we find that the probability of compounding associated with a cyclone class does not depend monotonically on the probabilities of the individual contributing hazards, but also on the goodness of their temporal and spatial correspondence. Finally, we find warm conveyor belts and cold fronts to frequently co-occur with rain and wind, and rain and wave events, while particulate matter and heat events are not strongly associated with dynamical features. These results, which systematically associate various large-scale environments and dynamical features to different compound event types, have implications for forecasting and climate risk predictions.

1 Introduction

Mediterranean cyclones are comprised of about 90% of extratropical-like and 10% of tropical-like cyclones (Emanuel, 2005; Miglietta, 2019; Flaounas et al., 2022). They constitute a distinct group of storms which are typically smaller and weaker than their oceanic counterparts (Flaounas et al., 2015, 2022). Still, the Mediterranean basin is one of the most active cyclogenetic regions of the world (Ulbrich et al., 2009), and the Mediterranean cyclones are associated with most of the high wind and precipitation impact throughout the region (Flaounas et al., 2022). In addition to heavy precipitation (Pfahl and Wernli, 2012; Flaounas et al., 2018) and high winds (Nissen et al., 2014), Mediterranean cyclones are associated with a broad variety of hazards ranging from sea waves (Cavaleri et al., 2012; Patlakas et al., 2021) to particulate matter (pm10) uplift and transport (Dayan et al., 2008; Kalkstein et al., 2020), and impacting many aspects of society.

Individually, such hazards certainly pose a risk to society, but recent research shows that the comparatively little studied compound events, may be responsible for an even larger fraction of the major climate and weather catastrophes impacting our societies (Zscheischler et al., 2018). Multivariate compound events, defined as events where the co-occurrence of hazards leads to higher impacts than any individual hazard would have caused (Zscheischler et al., 2020), have been shown to occur in the Mediterranean. Among others, wind and precipitation compound events (Raveh-Rubin and Wernli, 2015; Martius et al., 2016; Catto and Dowdy, 2021), sea waves and precipitation events (Bevacqua et al., 2019; Amores et al., 2020), and heat and pm10 events (Katsouyanni et al., 1993) have been observed in the region, and have been shown to impact infrastructure (wind,

https://doi.org/10.5194/egusphere-2023-2322
Preprint. Discussion started: 17 October 2023

precipitation and waves) and public health (pm10 and heat). Contrarily to individual hazards, the relation between compound hazards and Mediterranean cyclones has yet to be systematically characterized. Such a characterization is important, not only for the evaluation of climate risk (Bevacqua et al., 2019), but also to improve forecasting at shorter time scales (Saleh et al., 2017).

Additionally, within individual cyclones, hazards tend to occur in relation with dynamical features such as fronts (Dowdy and Catto, 2017), warm conveyor belts (WCBs, Flaounas et al., 2018) and dry intrusion (DIs, Raveh-Rubin, 2017). Quantifying this relation provides valuable information on the smaller-scale processes involved in the occurrence of hazards. Similar to the relation between the hazards and the cyclones themselves, the role of dynamical features in the Mediterranean has been investigated for individual hazards but not yet systematically for compound events. Previous efforts to quantify the relation between multivariate compound events, extratropical cyclones and dynamical features elsewhere in the world [citation of currently embargoed thesis by Laura Owen] are unlikely to provide much information applicable to the Mediterranean basin. This is the case because the sharp topography enclosing the small Mediterranean basin makes it a distinct and complex environment which can't be directly compared to large ocean basins (Flaounas et al., 2022). Notably, an important cyclone characteristic which emerges from the Mediterranean basin configuration is that the genesis and intensity of Mediterranean cyclones is typically controlled by the upper-level PV structure (Flocas, 2000) except in the rare tropical-like cyclones, where low-level PV generation is important (Flaounas et al., 2015). Even in less complex ocean basins, interactions accross scales mean that a dizzying variety of atmospheric configurations may give rise to high impact events. For that reason, a climatology of storm-related hazards in the Mediterranean must include information on the atmospheric configuration at multiple scales and levels, from upper-level synoptic scale flow, to surface dynamical features.

Hence, as a first step in characterizing the relation between compound hazards and Mediterranean cyclones, we aim to establish a storm-relative climatology of various compound events and the associated synoptic- and meso-scale dynamical features. Such a climatology

1. provides information on the spatial footprints of the compound hazards associated with the cyclones and on the seasonality of the link between cyclones and compound events;
2. clarifies the role of the large scale dynamics in setting conditions conducive to the occurrence of particularly impactful cyclones; and
3. quantifies the relation between smaller-scale dynamical processes and the occurrence of compound events, to disentangle the contribution at various scales to the occurrence of compound events.

This Lagrangian climatology focuses on three types of multivariate compound events, namely the co-occurrences of strong winds and heavy precipitation, of heavy precipitation and high sea waves, and of high pm10 concentration and heat waves. Hereafter these will be referred to as “rain-wind”, “rain-waves” and “pm10-heat” events. Studying these multivariate compound

https://doi.org/10.5194/egusphere-2023-2322
Preprint. Discussion started: 17 October 2023

hazards requires evaluating the occurrence of five individual hazards within a single consistent framework, so this study also incidentally provides a novel unified comparison of multiple single hazards associated with Mediterranean cyclones. Hence the occurrence of these five individual hazards is also analyzed, albeit in less detail than the compound events. Finally, the occurrence of three different dynamical features is analyzed in relation to the hazards: cold fronts (CF), warm conveyor belts and dry intrusions.

First, section 2 presents the methodology and data used in defining events and establishing the climatology, then section 3 presents summary results for the hazards and selected in depth analyses, and section 4 discusses mechanisms of compounding and compound event co-occurrence with dynamical features. A conclusion then synthesizes the study and introduces future areas of research.

2 Data and methods

The data required to establish this storm-relative climatology of compound hazards in Mediterranean cyclones is comprised of three different sets: 1) cyclone tracks to provide information on the location, timing and intensity of storms, 2) gridded datasets of individual hazards and 3) gridded datasets of dynamical features. The main methods required to process that data include 1) definitions of single-hazard and multivariate events, 2) compositing methods to characterize the occurrence of compound events and the co-occurence of events and dynamical features in the vicinity of storms, and 3) significance testing. The description of these datasets and methods follows.

2.1 Cyclone tracks and classification

To evaluate the relationship between compound hazards and Mediterranean cyclones, we use the storm tracks produced by the MedCyclones COST action, a coordinated initiative aiming to address unsolved questions regarding the dynamics, climatology and impacts of Mediterranean cyclones. This storm track dataset represents a best guess at the cyclones' position and pressure intensity throughout their life cycle. The best guess is obtained by averaging multiple separate tracking methods (Flaounas et al., 2023), relying on variables such as pressure minima and gradients, low-level relative vorticity, and geopotential. The tracks are computed using ERA5 reanalysis data (Flaounas et al., 2023), the high spatial and temporal resolutions of which leads to accurate tracking of storm centers (Aragão and Porcù, 2022). Figure 1 shows the average track density per year of all the tracks of the MedCyclones dataset. The figure outlines hotspots of storm activity around Italy and southern France as well as over the Sahara and south of Turkey. In general, there is more storm activity over bodies of water than over land, especially near the Northern shore of the Mediterranean.

To clarify the large-scale context within which the cyclones and the associated compound events occur, we use the upper-level potential vorticity (PV) classification of Mediterranean cyclones introduced by Givon et al. (2023). In this classification,

https://doi.org/10.5194/egusphere-2023-2322
Preprint. Discussion started: 17 October 2023

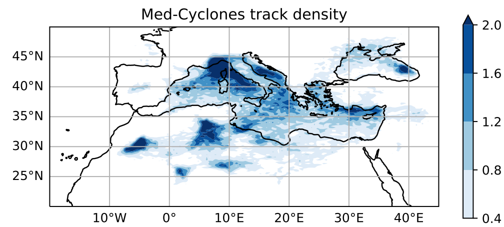

Figure 1. Density of cyclone tracks in the Mediterranean basin: average number of storms per year per 1×1 degree box. Note that this represents only the average number of storm centers tracked at a given location per year, not the much higher average number of different cyclones which impact that location.

the cyclones are organized into nine clusters based on the surrounding PV field averaged over the 320-to-340 K dry isentropic levels at the time of minimum central pressure, and using self-organizing maps (SOMs, Kohonen, 1990). The resulting similarity maps for all nine clusters, as well as the associated mean PV fields can be viewed in Figs. X and Y of Givon et al. (2023). In the present paper, only the large scale environment of storm clusters shown to be responsible for compound events will be discussed.

2.2 Hazard datasets

The wind, precipitation, wave height and heat wave data used to define single- and compound hazards are obtained from hourly-resolved ERA5 reanalysis (Hersbach et al., 2020), but only saved at 6h intervals for storage space economy. The wind variable is taken to be the magnitude of the 10-m wind components, which includes eastward and northward winds ("u10" and "v10" respectively in ERA5). We note that these represents grid-cell average winds which have smaller variability than observations. The ERA5 total precipitation variable used ("TP"), represents the 1-hour accumulated grid-cell average precipitation. This variable does not directly assimilate precipitation observations, but instead represents a short-term forecast initialized by the reanalysis (Hennermann and Berrisford, 2020), which has been shown to compare favorably to extreme precipitation in the mid-latitudes (Rivoire et al., 2021). The wave variable used here is the "significant height of combined wind waves and swell" ("swh"), which represents the average height of the highest third of waves associated with wind and swell. This variable can serve to assess the damage and flooding potential of the waves. Next, the temperature variable considered to assess the compounded impacts of dust and heat on human health is the temperature at two meters above ground ("t2m"). Finally, we use near-surface particulate matter at diameters lower than 10 μm ("pm10"), provided by the Copernicus Atmosphere Monitoring Service (CAMS) reanalysis (Inness et al., 2019). The CAMS pm10 variable compares very well with surface observations of particulate matter over Europe (Rémy et al., 2019). We note that, even though pm10 combines multiple aerosol types at diameters less than 10 μm, the majority of the concentration around the Mediterranean basin is due to dust particles, the main

https://doi.org/10.5194/egusphere-2023-2322
Preprint. Discussion started: 17 October 2023

source of which is the Sahara (Rémy et al., 2019). Hence, here we will consider that the origin of high pm10 events is usually the emission and transport of Saharan dust.

2.3 Dynamical features datasets

The dynamical features datasets used here were introduced in previous studies, and kindly made available to us. These include a dataset of objectively identified front lines (introduced by Catto and Pfahl, 2013) computed using ERA-Interim reanalysis, a dataset of DI trajectory density (introduced by Raveh-Rubin, 2017) also computed using ERA-Interim reanalysis and a dataset of WCB trajectory density (Heitmann et al., 2023) computed using ERA5 reanalysis data. Note that the methods used to identify DIs and WCBs are similar, while the front identification method is very distinct. This must be taken into account when assessing the co-occurrence of hazard events with dynamical features.

2.4 Event definition

In this study, the occurrence of a multivariate compound event is defined as the co-occurrence of two single-hazard events, as was done in previous literature such as [citation of currently embargoed thesis by Laura Owen]. Single-hazard events are defined as the exceedance of a threshold chosen to represent a given level of risk. Risk depends not only upon the magnitude of the hazard but also upon the local vulnerability to that hazard, which may have large spatial variability. When that is the case, a given hazard magnitude may be benign in one region and catastrophic in another, and local percentile thresholds are most appropriate to capture the local risk. Otherwise, a fixed threshold may be used to define the occurrence of events everywhere.

The vulnerability to the precipitation hazard is highly variable spatially and, following previous literature (e.g., Catto and Pfahl, 2013), we choose the 99^{th} percentile as a threshold for the occurrence of an event. In addition, since our analysis domain includes very arid regions like the Sahara, we seek to avoid considering trace precipitation as rain events. To do so, we add another criterion to the event threshold, which is that the 1-hour integrated precipitation must also exceed 1 mm to be considered an event. In other words $T_p = \max(99^{th}, 1 \text{ mm/h})$, where T_p is the precipitation event threshold. Similarly, the vulnerability to wind damage is variable in space, and in keeping with previous literature, we select the 98^{th} percentile of wind magnitude (Klawa and Ulbrich, 2003), along with a fixed minimum threshold of 10 m s^{-1} to yield a wind threshold $T_w = \max(98^{th}, 10 \text{ m s}^{-1})$. Figure 2 shows maps of the precipitation and wind thresholds used in this study. The top panel shows that wind thresholds are highest over bodies of water and coastlines, except in particularly windy locations such as Chad (at the Bodele depression) or Iceland. The bottom panel shows that precipitation thresholds are typically highest downwind of large bodies of water, in mountainous regions and interestingly, wherever Mediterranean cyclone track density is high (see Fig.1). At the same time, they are very low in subtropical subsidence regions such as the Sahara and the Arabian Peninsula. Note that the domain presented in Fig.2 is larger than that within which Mediterranean cyclones are tracked (shown in Fig.1) so that compositing is possible around cyclones occurring on the edge of the Mediterranean basin.

https://doi.org/10.5194/egusphere-2023-2322
Preprint. Discussion started: 17 October 2023

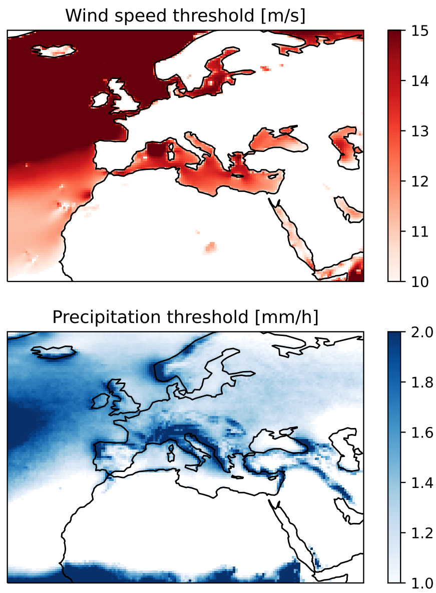

Figure 2. Maps of winds and wind threshold

The threshold for waves is taken here to be fixed at 4 m because that is a representative value for the 99^{th} percentile of significant wave height (e.g., Barbariol et al., 2021, Fig.5) and close to the significant wave height observed in damaging storms (e.g., Amores et al., 2020). This is reasonable since there does not seem to be an agreed-upon definition of space-varying wave event threshold, and percentile maps are not as variable for waves as they are for precipitation or winds. In the case of pm10, high concentrations may pose health risks anywhere and a fixed threshold is chosen. We select a 50 μg m^{-3}, 24-h averaged threshold, equivalent to the recommendation of the European union for 24h exposure to pm10 (EU and Parliament, 2008) and 10% higher than the World Health Organization recommendation (WHO and for Environment, 2021). Finally, for heat events, we chose a fixed 30 C threshold to be consistent with previous studies of increased mortality in the event of co-occurring dust and heat extremes (Katsouyanni et al., 1993). We note that since empirical quantiles are not defined for multivariate distributions, defining compound events as the co-occurrence of single-hazard events circumvents having to fit a copula to the multivariate distribution of hazards, and hence offers a bit more flexibility in defining such events.

2.4.1 Dynamical features occurrence

The criterion to define whether warm conveyor belts or dry intrusions are present at a given gridpoint is taken to be the presence of a non-zero WCB or DI trajectory density at that gridpoint. Here, WCB trajectories are assumed to be important for surface

https://doi.org/10.5194/egusphere-2023-2322
Preprint. Discussion started: 17 October 2023

hazards only between the surface and a pressure of 400 hPa, so WCB trajectory density at upper levels is not considered. WCB and DI trajectory density data is 2-dimensional (2D), so it can be directly compared to 2D hazard data. On the other hand, in the dataset we are using, fronts are defined as 1D features (Catto and Pfahl, 2013). To assess the role that fronts may have in the occurrence of hazards, a "zone of influence" must be defined and the 1D features must be transformed into 2D maps. Following previous literature (e.g., Catto and Pfahl, 2013) any location within 2.5 degrees of a point where a front is located is deemed to be potentially influenced by that front.

2.5 Compositing

The storm-relative composites are obtained by first evaluating the occurrence of single-hazard events for all variables, in a 40×40 degrees box centered on each cyclone, only at the time of minimum central pressure. Since the time resolution of the storm tracks is sometimes higher than that of the hazard data, we select the minimum pressure over the times when hazard data is available. Selecting a single snapshot per storm removes any ambiguity in separating events or in evaluating the contribution of each storm to the final composite [citation of currently embargoed thesis by Laura Owen]. The hazard data is linearly interpolated onto the storm box, at a 0.25 degrees resolution, as is the hazard threshold if it is variable in space (precipitation and winds). Event occurrence is then computed, yielding one 2D boolean matrix per storm and per hazard, with storm-relative latitude and longitude, indicating where an event is detected (value of 1) and where no event is detected (value of 0). These matrices are produced for all cyclones and then stacked into one 3D boolean matrix per hazard with dimensions Storm ID, storm-relative longitude and storm-relative latitude. This is illustrated on the top row of Fig.3, where colored cells indicate hazard threshold exceedance (value of 1) and white cells indicate no threshold exceedance (value of 0). The composites of individual hazard frequency are obtained by averaging these matrices along the Cyclone ID dimension.

2.5.1 Co-occurrence analysis

To evaluate the occurrence of multivariate compound hazards, one simply needs to compute the co-occurrence of individual hazards by taking the intersection of individual hazard boolean matrices. In Figure 3, the bottom left panel illustrates the result of computing the compounding of Hazard A and Hazard B (top row). The main thing to notice is that the area of compound events is smaller than that of either individual hazard and that its shape is determined by the overlap of the individual hazard footprints. The final step to obtain storm-relative composites of compound events is to take the average of the boolean compound matrix along the Storm ID dimension (Fig. 3, bottom right). This yields storm-relative maps of compound event occurrence probabilities, with values between 0 (never occurs in the storm sample) and 1 (always occurs in the storm sample).

2.5.2 Masked compositing

In the case where we composite hazards which are not defined everywhere, such as waves which only happen in the sea, we need to proceed a bit differently. Storms are only included in the composite if their centers are over the Mediterranean at the time of minimum pressure, and all land points as well as the Atlantic Ocean are masked out and are discounted in the averaging

https://doi.org/10.5194/egusphere-2023-2322
Preprint. Discussion started: 17 October 2023

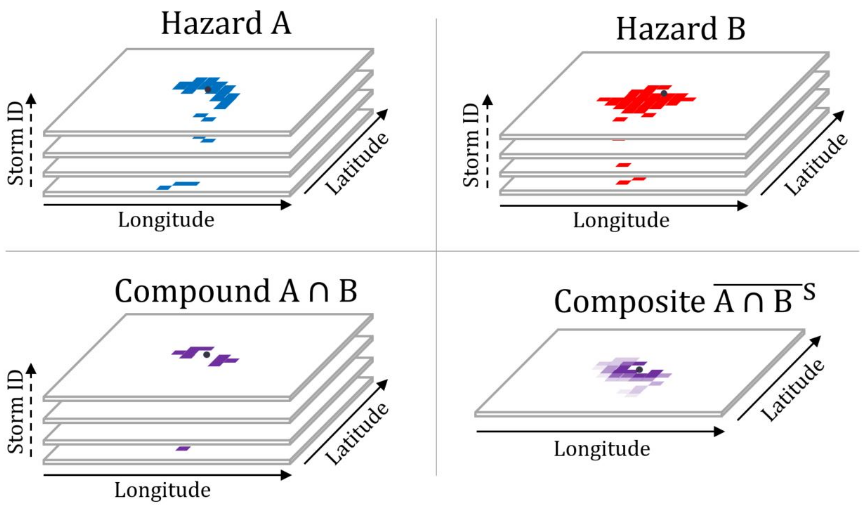

Figure 3. Boolean matrices of event occurrence for individual hazards (Hazards A and B), with dimensions Cyclone ID, and storm-relative horizontal coordinates. Colors (blue and red) indicate event occurrence (1) and white space indicate non-occurrence (0). Boolean matrix of compound events (Compound $A \cap B$) obtained by taking the intersection of Hazard A and Hazard B (purple). Matrix of compound event probabilities (Composite $\overline{A \cap B}^S$) obtained by averaging the compound event matrix across the Storm ID dimension. Darker shades of purple indicate higher probabilities (maximum 1) and lighter shades indicate lower probabilities (minimum 0).

of the 3D occurrence matrices to obtain composites. This means that a spatially varying number of different storms is used in computing the final storm composite map. The number of data points available for compositing tends to decrease away from the storm center, which mean that the data there is less reliable. This is accounted for in the significance testing; locations where there are too few points are not found to be significant.

2.6 Significance testing

The compositing step yields a storm-relative map of compound event probabilities. To assess the statistical significance of each point constituting the map, we aim to test the null hypothesis that the probabilities of compounding associated with storm events is not different from the probabilities of compound events at all times at that point. To that end, we produce Monte-Carlo samples of hazard events at the same locations as those of the storm samples, but at random times. Albeit random, the times are selected to yield the same seasonal distribution as that of the storm sample (e.g., Welker et al., 2014). We produce 2000 such Monte-Carlo samples for each hazard, which are used to compute 2000 maps of compound hazard probabilities. Empirical p-values are then computed at each point of the storm-relative maps of compound hazard probabilities as one minus the quantile of that point within the corresponding Monte-Carlo samples. If the probability at the storm point is the largest, it is attributed a p-value of 0. When evaluating a large number of significance tests, it becomes problematic to reject the null hypothesis based upon a fixed threshold for the p-value (Wilks, 2016). Hence, following Wilks (2016), we control for the false

https://doi.org/10.5194/egusphere-2023-2322
Preprint. Discussion started: 17 October 2023

discovery rate by sorting all N empirical p-values in ascending order, from p_1 to p_N and by computing an effective p-value significance threshold p_{fdr} given by

$$p_{fdr} = \max_i \left(p_i \;\middle|\; p_i \leq \alpha \frac{i}{N} \right) \tag{1}$$

where $\alpha = 0.05$ is the false discovery rate control level (Wilks, 2016)). In practice, in our analyses, p_{fdr} is around 0.005, which is considerably more constraining than a typical 0.05 threshold.

3 Results

For brevity, we do not show the storm-relative footprints of five single hazards and three types of multivariate compounding for all nine storm clusters. We first present compact summaries of the risk associated with each hazard and each compounding type in each cluster. These summaries are then used to determine which storm clusters are worthy of note in the context of the different types of multivariate compounding analyzed here. Once the most important cyclone clusters are identified, their compounding structure as well as their large scale context is discussed. To summarize the risk associated with a (single or compound) hazard within a given cluster, we average the hazard probabilities over a 20×20 degrees box centered on the storm composite for that cluster. Probabilities that are not statistically significant are set to zero in this averaging process. In that analysis, storms that either have a points with higher hazard probabilities or a larger hazard footprint are found to be associated with higher risk. Setting the probabilities of non-significant points to zero ensures that clusters for which the probability of a hazard has no field significance will be found to have zero risk associated with that hazard. If we consider Boolean matrices as binary matrices, the summary metrics for single and compound hazards are computed as

$$P_A = \overline{A}^{SH}, \quad P_C = \overline{\min(A,B)}^{SH}, \tag{2}$$

Where A and B are two different hazards, the overline denotes an average, and S and H are respectively the "Storm ID" and the horizontal (latitude-longitude) dimensions of a 20×20 degree box around the cluster center. P_A and P_C are respectively the probabilities of hazard A and compound hazard A-B, which may be interpreted as the fraction of time a compound event will occur at any point within a 20×20 degrees box centered on a Mediterranean cyclone. Note that the probabilities of different hazards or clusters are more meaningful relative to one-another than considered independently because the size of the averaging box influences their absolute value. Doubling the area of the averaging box would lead to a halving of all average probabilities, as long as all statistically significant points are encompassed within both boxes.

3.1 Individual and compound hazards overview

First, figure 4 shows the averaged probability of occurrence for the rain hazard, the wind hazard and the compounding of both winds and rain. Each bar of the plot represents a different cluster, and the clusters are sorted by average compound risk, in

https://doi.org/10.5194/egusphere-2023-2322
Preprint. Discussion started: 17 October 2023

decreasing order. The average compound event probability exhibits large differences between clusters, with three clusters (2, 4 and 1) being responsible for the majority of the rain and wind compound risk. These clusters are associated with higher compound risk to infrastructure and will be investigated in more detail. Cluster 6 is not associated with any statistically significant occurrence of compound events despite being associated with small but statistically significant rain events and wind events. This leads us to the observation that rain-wind compound probabilities are systematically multiple times smaller than either rain probabilities or wind probabilities alone. Further, while the probability of compounding scales approximately with the probabilities of individual hazards, there are cases where lower probabilities of individual hazards are associated with higher probabilities of compounding. Notably, cluster 2 which exhibits the highest compounding probabilities, has lower individual probabilities of both precipitation and wind events than cluster 4. We will return to this result in section 4.

Next, figure 5 shows the averaged probability of rain hazard, wave hazard and the compounding of both rain and waves. Note that the rain probabilities are computed only over the sea here and, in order to be more directly comparable, are masked in the same way as the wave events. As a result, the rain probabilities shown here are slightly different than the ones shown in Fig.4. For example cluster 6 is not associated with any statistically significant precipitation over the sea because storms in that cluster occur almost exclusively over land (Givon et al., 2023). Here, only three clusters (2, 4 and 8) are associated with statistically significant compound flooding risk. Note that cluster 1 compound event probability is not significant despite the associated wave event probability being higher than that of cluster 8.

Finally, figure 6 shows the averaged probabilities of pm10 hazard, heat hazard and the compounding of both pm10 and heat. Once again, most of the compound events are concentrated within a few clusters which pose a higher risk to public health (6, 7 and 5), with some clusters exhibiting no significant compositing (2, 4 and 1). This time however, by contrast to the rain-wind and rain-waves compound types, there is no clear scaling of the compound event probability with the individual hazard probabilities. Note the case of cluster 2,4? which is associated with the highest pm10 probability but no statistically significant heat or compound event probability. Interestingly, there is little overlap between the clusters that are important for pm10-heat events, and the clusters responsible for both rain-wind events and rain-wave events. In fact, none of the clusters most important for wind and rain compositing (2, 4 and 1) are associated with heat event field significance.

3.2 Geographical, seasonal and dynamical context of clusters of interest

Based on the summary of compound event probabilities (Figs.4-6), we select for further analysis the three clusters which are most important for each type of compounding. Weighting by the relative number of storms tracked in each cluster (Givon et al., 2023), the clusters 2, 4 and 1 collectively account for 79% of rain-wind events, cluster 2, 4 and 8 account for all rain-wave

https://doi.org/10.5194/egusphere-2023-2322
Preprint. Discussion started: 17 October 2023

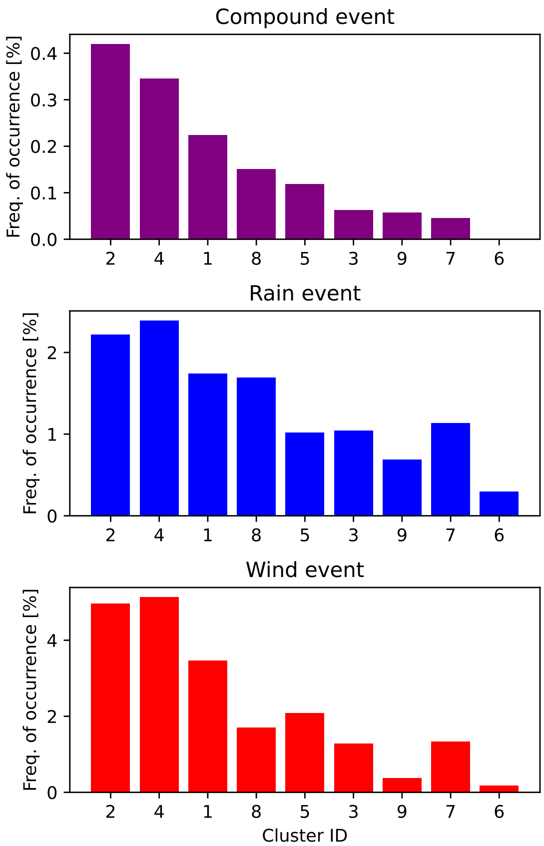

Figure 4. Risk summary for all clusters for rain and wind compounding (top panel, purple bars), for rain alone (middle panel, blue bars) and for wind alone (bottom panel, red bars). The clusters are plotted in decreasing order of compound risk, for all panels.

events, and clusters 6, 7 and 5 account for 80$\%$ of pm10-heat events. These high percentages warrant focusing further analyses on the three clusters selected as most important for each compounding type. Figure 7 shows the spatial density and seasonal cycle of storms at the time of minimum central pressure (used in compositing), which provides insight on the geographical and seasonal context within which cyclones associated with compound events occur. Note that overall, the density plots capture similar high-density areas as Fig.1, which represented the density of tracks at all times. First, the density of events associated with rain-wind compounding is highest around Corsica and northern Italy, and is generally high along the north shore of the Mediterranean. The absence of rain-wind compound storms in the south is consistent with the seasonal cycle of these storms, which peaks markedly in winter, and craters to zero in mid-to-late summer. Since there is a single different cluster, the geo-

https://doi.org/10.5194/egusphere-2023-2322
Preprint. Discussion started: 17 October 2023

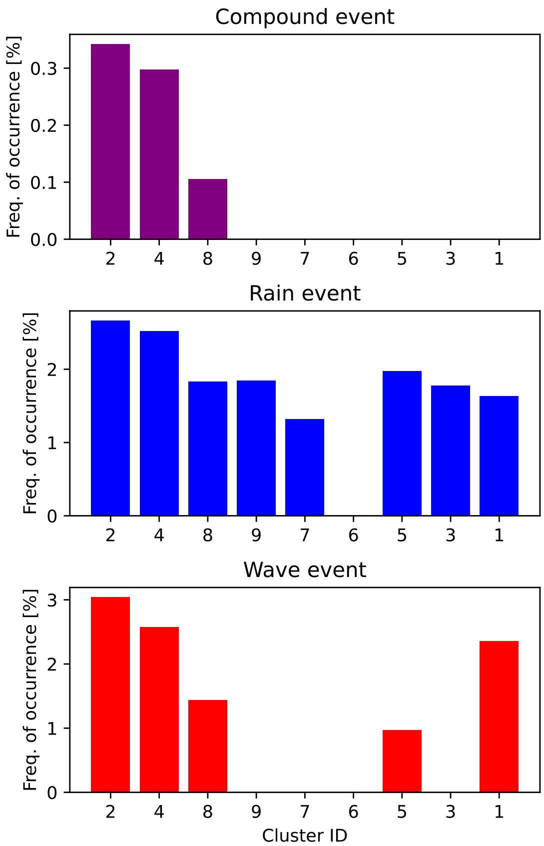

Figure 5. Risk summary for all clusters for rain and waves compounding (top panel, purple bars), for rain alone (middle panel, blue bars) and for waves alone (bottom panel, red bars). The clusters are plotted in decreasing order of compound risk, for all panels.

graphical and seasonal distribution of rain-wave storms is very similar to that of rain-wind storms. The main spatial density differences are that rain-wave storms are a bit less dense around northern Italy, and a bit more around Cyprus, as well as occurring occasionally further south. The seasonal cycle of rain-wave storms plateaus in winter and early spring before decreasing to a minimum in summer and re-increasing through fall. Finally, pm10-heat storms occur much more to the south than other clusters, especially over Morocco and Algeria, but still occur occasionally throughout the Mediterranean basin. Correspondingly, these storms occur least in winter, increase in early spring, plateau through summer, and decrease during the fall. The differences in seasonality and spatial distribution of the clusters associated with rain-wind and rain wave events on the one hand, and pm10-heat events on the other hand warrants the partition of Mediterranean cyclones into clusters, which can be

https://doi.org/10.5194/egusphere-2023-2322
Preprint. Discussion started: 17 October 2023

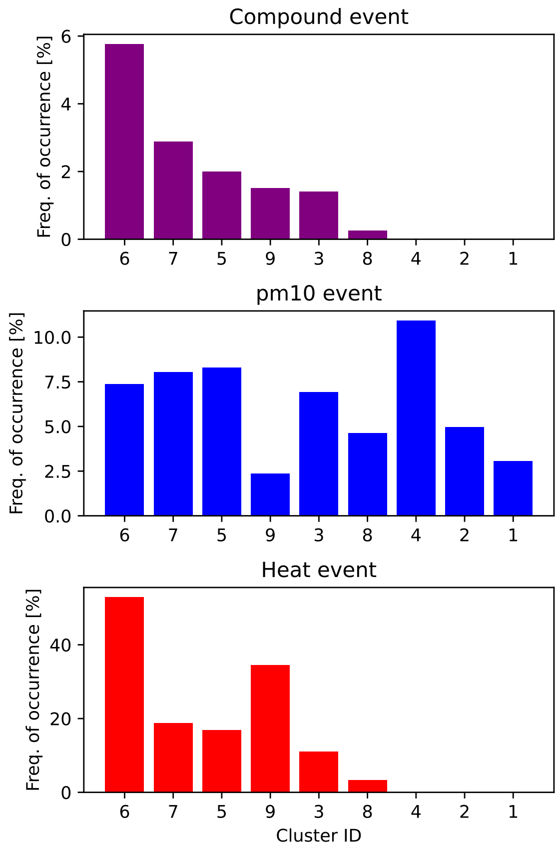

Figure 6. Risk summary for all clusters for pm10 and heat compounding (top panel, purple bars), for pm10 alone (middle panel, blue bars) and for heat alone (bottom panel, red bars). The clusters are plotted in decreasing order of compound risk, for all panels.

studied separately for more accurate insight into specific compound hazards.

295 Figure 8 shows maps of upper-level potential vorticity and sea-level pressure for clusters of interest as a means to clarify the large-scale dynamical context within which compound events occur in Mediterranean cyclones (Givon et al., 2023). Maps are shown for the clusters responsible for most of the compound event risk, omitting cluster 1 for brevity, because it is similar to cluster 4. In the PV-based classification, the cluster 4 composite is interpreted as a paradigmatic example of type B frontal cyclones (Petterssen and Smebye, 1971), and its structure is similar to that associated with the most intense cyclones in the

https://doi.org/10.5194/egusphere-2023-2322
Preprint. Discussion started: 17 October 2023

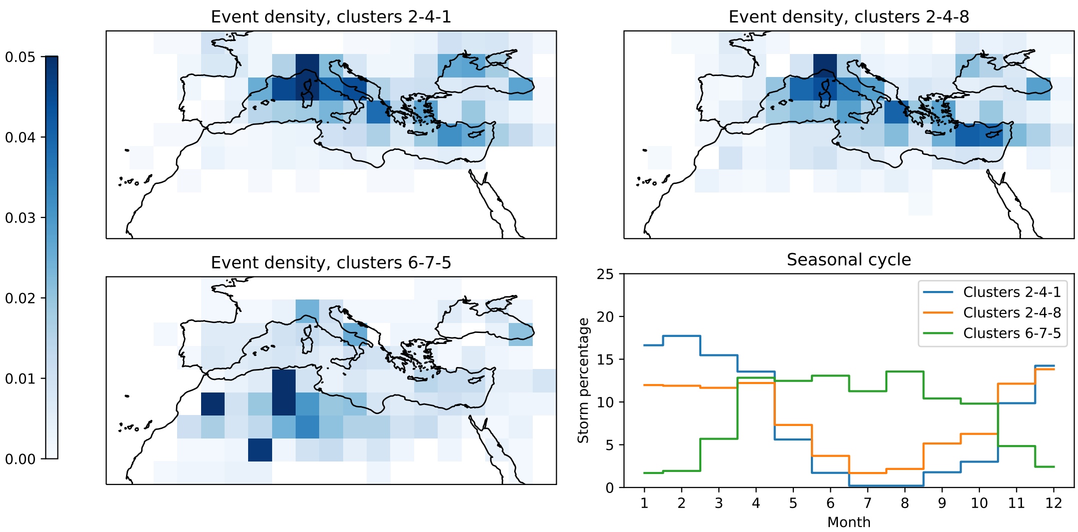

Figure 7. Cyclone event density for the clusters associated with rain-wind events (top left, clusters 2-4-1), with rain-wave events (top right, clusters 2-4-8) and with pm10-heat events (bottom left, clusters 6-7-5). Seasonal cycles of cyclones associated with the three compounding types (bottom right).

Mediterranean (Flaounas et al., 2015). Cluster 1 cyclones, which are quite similar, are interpreted as slightly weaker type A cyclones (Petterssen and Smebye, 1971). Clusters 2 and 5 are both considered cases of anticyclonic wave breaking (AWB, Thorncroft et al., 1993), albeit occurring mainly in the midlatitudes for cluster 2 and in the subtropics for cluster 5, while cluster 8 ORM TO ME ALSO ACWB, CL7 LOOKS CYCLONIC may be associated with cyclonic wave breaking (CWB, Thorncroft et al., 1993). Both AWB and CWB have been shown to be involved in Mediterranean cyclones (Flocas, 2000). Cluster 7 cyclones are interpreted as daughter cyclones forming in the warm sector of parent cyclones located to their north during transition seasons (potentially cyclones from clusters 1 or 2). These small scale and fast moving relatively dry cyclones often form in the lee of the Atlas and are associated with dust storms (Bou Karam et al., 2010). This is particularly interesting because it outlines that, in transition seasons, a given large-scale configuration may give rise simultaneously to rain-wind and pm10-heat events in different locations. Finally, cluster 6 cyclones, which are very weakly baroclinic, are interpreted as heat lows, and occur mainly in the Sahara in summer. To sum up, rain-wind events are predominantly associated with anticyclonic wave breaking and type A and B frontal cyclones, rain-wave events are additionally associated with cyclonic wave breaking, and pm10-heat events are associated with heat lows, daughter cyclones and anticyclonic wave breaking in the subtropics. Note that there are strong seasonal and geographic variations in the PV structure associated with cyclones in the Mediterranean (Givon et al., 2023). For that reason, while they outline the role of dynamics more, the results obtained using a PV-based classification are likely similar to the results one would obtain using geographical and seasonal classifications, and must be interpreted in that context. For example, despite similar upper level configurations, the very different regions within which

https://doi.org/10.5194/egusphere-2023-2322
Preprint. Discussion started: 17 October 2023

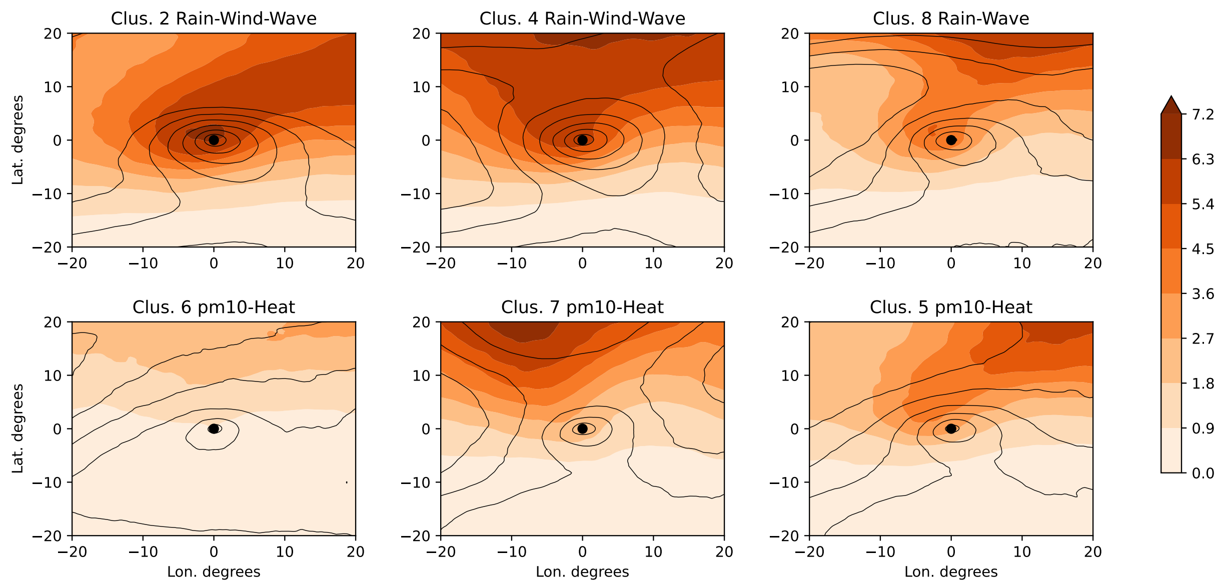

Figure 8. Large scale environment associated with clusters 2, 4, 8, 6, 7, and 5. The upper-level environment is represented by contours of potential vorticity averaged over the 320-340 isentropes (Orange filled contours), and the surface environment is represented by contours of potential? sea-level pressure (black contours at 250 Pa intervals).

cluster 2 and 5 storms occur largely influence the hazards with which they are associated (pm10 and heat for cluster 5, and wind, waves and precipitation for cluster 2).

3.3 Hazard footprints

Having discussed the context within which storms associated with compound event occur, we now examine the hazard footprint of the cyclones within clusters of interest. Starting with rain-wind events, Fig. 9 shows the storm-relative composite probability of occurrence for rain, wind and rain-wind events. Color shading shows the percentage of storms where a hazard event occurs at a given location and in a given cluster. The black contour encloses the statistically significant hazard area. As reported in previous literature [citation of currently embargoed thesis by Laura Owen], the distribution of individual events around the storm centers differs quite strongly between wind and rain events. Rain events are mostly concentrated to the north of the storm centers and the highest event probability is located to the northwest of the center. The wind event footprint, on the other hand, is much broader than that of rain, and mostly concentrated south of the center. Wind events occur most frequently south-south-west of the storm centers, and almost never immediately near the storm center. This sparsity of rain events around the storm centers in our composites shows that the location of the tracked center in the dataset used here (Flaounas et al., 2023) coincides well with the quiescent storm centers in ERA5 data. The probability of occurrence of events as defined here (see section 2) peaks at around 24% for rain and 30% for winds. The footprints also vary in both shape and magnitude across

https://doi.org/10.5194/egusphere-2023-2322
Preprint. Discussion started: 17 October 2023

clusters. Cluster 4, has and intense and broad rain footprint while cluster 2 has a smaller but equally intense footprint which is more concentrated to the northwest. Cluster 1 has the smallest and weakest rain footprint, but the statistically significant rain risk area extends further south than that of the other clusters. Wind events are most frequent and most concentrated to the south in cluster 4, while in cluster 2, and to a lesser extent cluster 1, the wind footprint wraps around the storm center to the west and up to the northwest. As a consequence of the very distinct areas occupied by the wind and rain event, compound events tend to occur less frequently than either individual events (peaking around a probability of 5%), and to be concentrated where both footprints overlap the most. In general, compound risk peaks to the west-north-west of the storm center, with a crown of (lower) risk encircling the storm center. Despite having somewhat smaller and weaker wind and rain footprints than cluster 4, cluster 2 is associated with the highest rain-wind compound risk.

Next, Fig. 10 shows the storm-relative composite probability of occurrence for rain, wave and rain-wave events. These composites are computed over the Mediterranean sea only. Both the land and the Atlantic Ocean are masked out from the averaging, and only storms that are over the sea at the time of minimum pressure are averaged in the composite. Masking out land and the ocean means that a small number of data points are used in the composites far from the storm center. There, the composite becomes very noisy, and hence, for ease of interpretation, locations where the hazard probabilities are not significant are left blank. Similarly to the rain and wind events, rain and wave events footprints vary widely between hazards and across clusters. Rain events over the sea tend to occur mostly north of the storm center, as is the case when rain over land is also considered (see Fig.4). Wave events occur most frequently to the west of storm centers. In clusters 2 and 4, the wave event footprints tend to extend to the northeast of the storm center. As a result, in these clusters, waves and rain events also co-occur most to the north of the event. Wave event probability peaks around 16% while rain-wave event probability peaks around 6%. Interestingly, the composite of rain events occurring only over sea does not exhibit much of a magnitude difference with the composite of all rain events. This can also be seen by comparing the “Rain event” graphs in Fig.4 and Fig. 5.

Finally, Fig. 11 shows storm-relative composites of pm10, heat and pm10-heat events. The pm10 events are fairly well distributed around cluster 6 cyclone centers, but peak a bit to the northeast. In clusters 7 and 5, however, the pm10 event probability footprint is located clearly to the south of the storm center, and stretches along a southwest-to-northeast axis reminiscent of a trailing frontal or conveyor belt structure. Heat event structure follows a north-to-south gradient and peaks at high values, above 50%. This is not surprising since these storms occur mostly in warm seasons and in warm regions (see Fig. 7). Cluster 6 is particularly hot and is associated with a majority of heat lows over the desert (Givon et al., 2023). In clusters 7 and 5, the deflection of the near-surface heat event frequencies associated with the storm is clearly visible, which outlines a possible role of Mediterranean cyclones in heat events. Note that the heat events are chosen here as exceeding the temperature above which heat effects on human health start to interact with dust concentration (Katsouyanni et al., 1993). They are not defined as a hazard in and of themselves, and should only be interpreted as such with some caution. For clusters 6 and 7, the

https://doi.org/10.5194/egusphere-2023-2322
Preprint. Discussion started: 17 October 2023

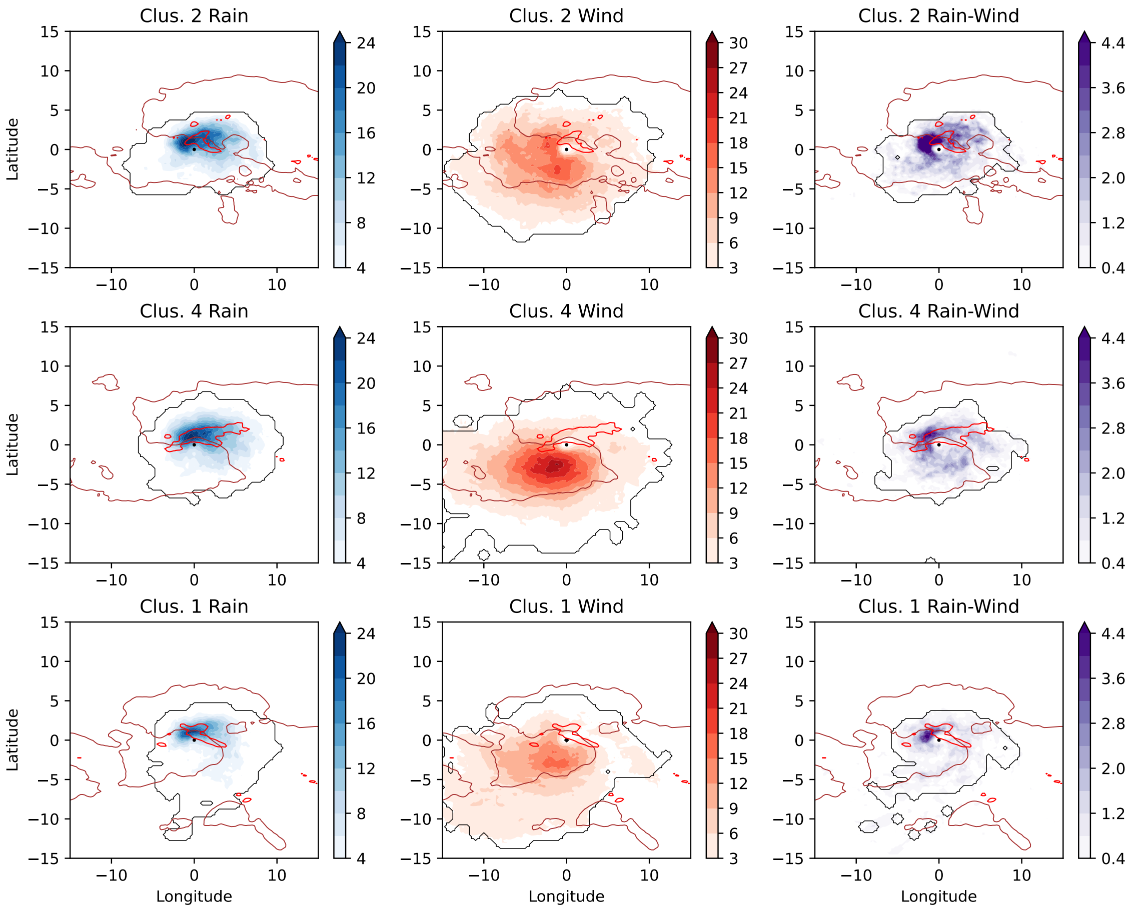

Figure 9. Storm-relative composite probability of rain events (blue shading, left column), wind events (red shading, center column) and compound rain-wind events (purple shading, right column) and for cluster 2 (top line), cluster 4 (middle line) and cluster 1 (bottom line). Probabilities are in %. The black contour identifies the statistically significant area for each hazard. The brown and red contours respectively identify the 300 m isohypse and the 100-m-per-degree meridional gradient of the storm-relative elevation composite.

compound pm10-heat footprints have a similar shape as the pm10 footprints, while it is displaced to the north in cluster 5. Note that the magnitude of the compound event probability is quite close to the pm10 probability in cluster 6, but much smaller for the two other clusters. This will be discussed in more detail in section 4.

https://doi.org/10.5194/egusphere-2023-2322
Preprint. Discussion started: 17 October 2023

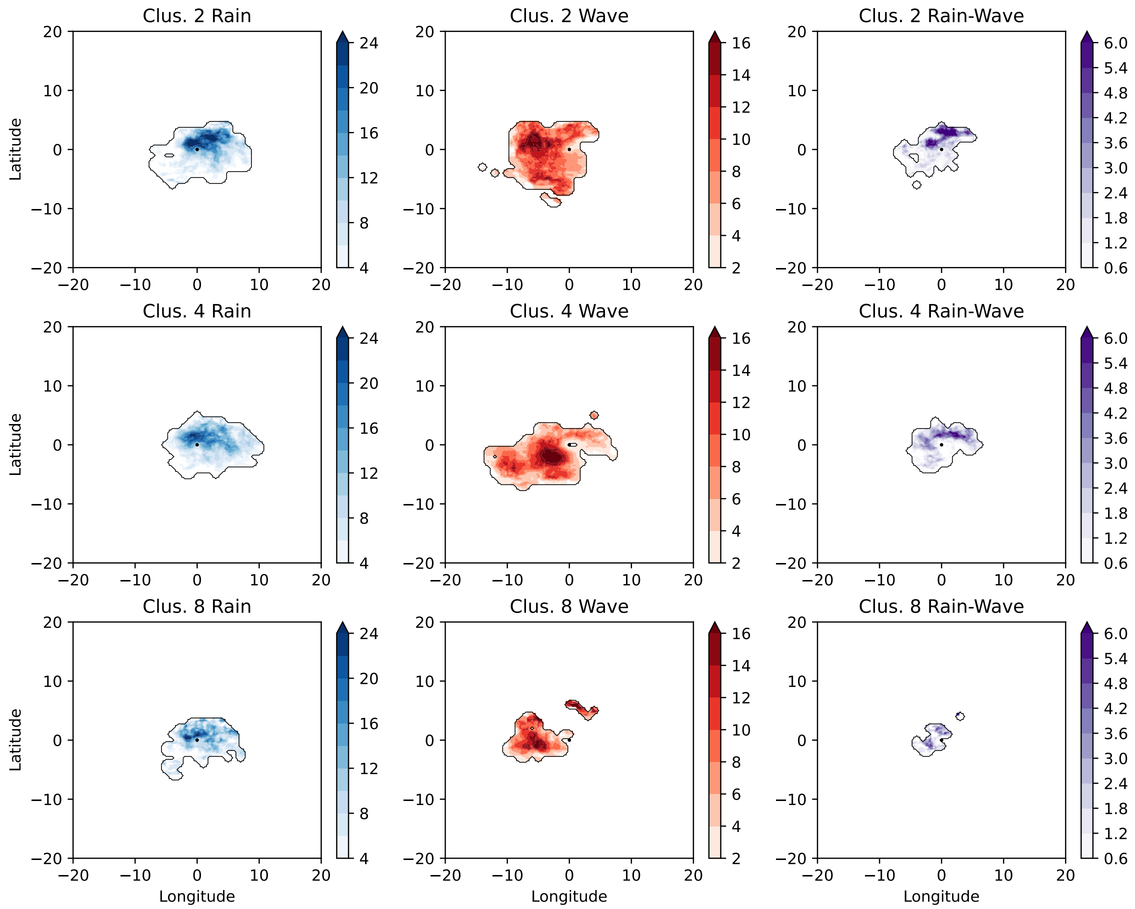

Figure 10. Storm-relative composite probability over the Mediterranean for rain events (blue shading, left column), wave events (red shading, center column) and compound rain-wave events (purple shading, right column) and for cluster 2 (top line), cluster 4 (middle line) and cluster 8 (bottom line). Probabilities are in %. The black contour identifies the statistically significant area for each hazard.

4 Discussion

4.1 Relation between individual hazard and compounding frequencies.

In Figs.9-11, we noted that, for rain-wind and rain-wave events, compound event probabilities usually scale with the probabilities of both constituting individual hazard. This is to be expected if the different individual hazards involved co-vary

https://doi.org/10.5194/egusphere-2023-2322
Preprint. Discussion started: 17 October 2023

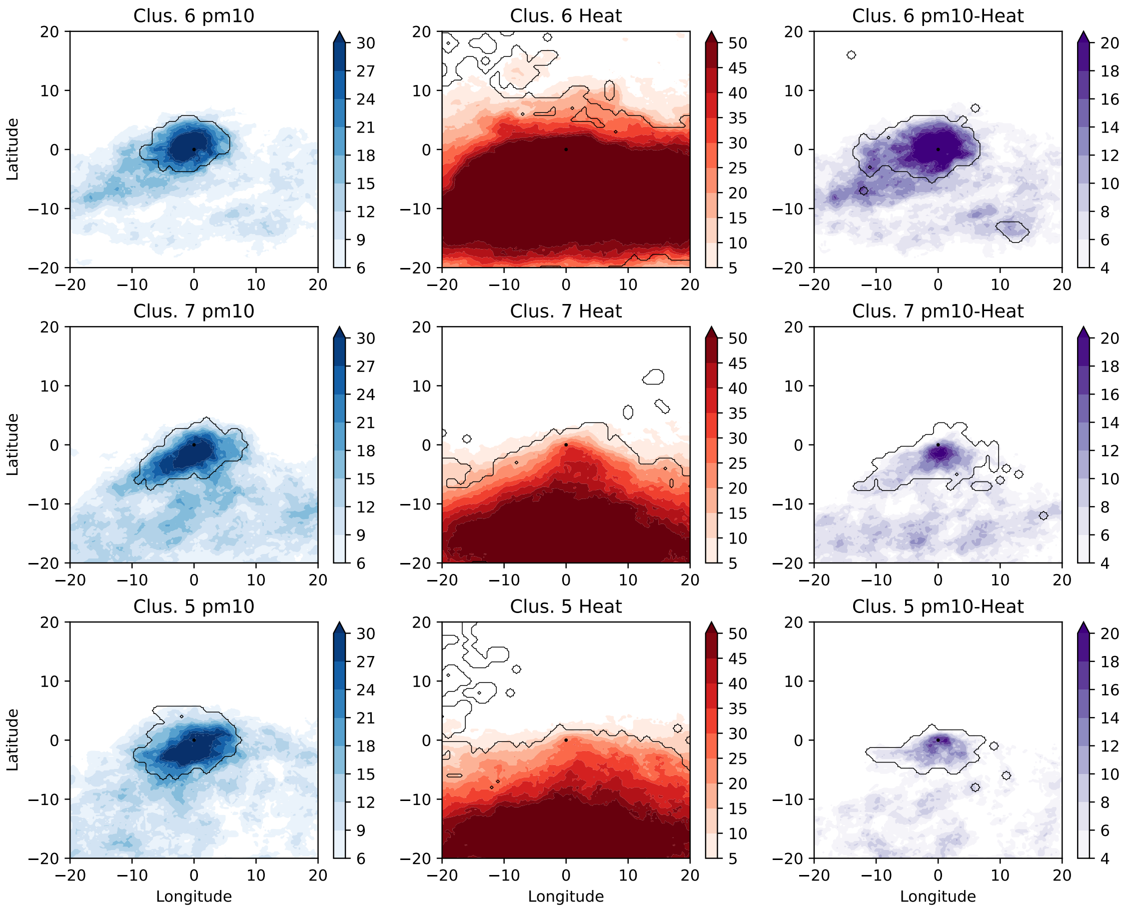

Figure 11. Storm-relative composite probability of pm10 events (blue shading, left column), heat events (red shading, center column) and compound pm10-heat events (purple shading, right column) and for cluster 6 (top line), cluster 7 (middle line) and cluster 5 (bottom line). Probabilities are in %. The black contour identifies the statistically significant area for each hazard.

and co-occur similarly across all clusters. Beyond such similarity across clusters, it becomes unclear how the temporal and structural characteristics of single hazards influence compounding. For example, wind footprint shape differences may be the reason why cluster 4, which is associated with higher probabilities of both rain and wind individual events than cluster 2, exhibits lower compound probabilities. Alternatively, clusters with very high pm10 probabilities frequently aren't associated with many heat events and vice-versa. Such variations make it difficult to intuitively understand why certain clusters are associated with higher probability of compounding, and hence higher risk. To help understand what sets the probability of compound

https://doi.org/10.5194/egusphere-2023-2322
Preprint. Discussion started: 17 October 2023

events in a given cluster, we start by quantifying the relation between the occurrence of individual events, and the occurrence of compound events. To do so, we introduce an "Ideal" compounding scenario, as well two co-occurrence metrics: "Simultaneity" and "Overlap". The Ideal scenario is a simple evaluation of the maximum compounding rate that could occur in a cluster if all the individual hazard events in that cluster were perfectly matched in space and across storms. Ideal compounding is defined as

$$P_I = \min(\overline{A}^{SH}, \overline{B}^{SH}), \quad (3)$$

where the overline denotes an average, and S and H are the storm event dimension and the horizontal dimensions respectively. As in Eq.2, the horizontal average is taken over a 20×20 degrees box. Using Eq.2, this formulation is equivalent to $P_I = \min(P_A, P_B)$. The left column of figure 12 shows the comparison between the ideal P_I and the actual P_C compound event probabilities. The actual probability of events is much smaller than the ideal probability for both the rain-wind and rain-wave events, but not for the pm10-heat events. As suggested before, the ideal rain-wind compound probability of cluster 4 is larger than that of cluster 2 despite the actual probability being smaller. Similarly, the ideal pm10-heat probability of clusters 7 and 5 is higher than that of cluster 6 event though cluster 6 has the highest actual compound event probability. In fact, for cluster 6, the actual probability is almost as large as the ideal probability. To understand the disparities between ideal and actual compound probabilities, we now turn to Simultaneity (Sim.), a measure of the extent to which different individual hazards tend to occur in the same cyclones within a cluster, and Overlap (Over.), a measure of how well individual hazard footprints correspond in space. Simultaneity and Overlap both vary between 0 and 1 and are given by

$$Sim = \frac{P_C}{\overline{\min(\overline{A}^{S}, \overline{B}^{S})}^{H}}, \quad (4)$$

$$Over = \frac{P_C}{\overline{\min(\overline{A}^{H}, \overline{B}^{H})}^{S}}, \quad (5)$$

where P_C is defined as in Eq.2. The right column of figure 12 shows that, Overlap is smaller in cluster 4 than in cluster 2, which finally explains the smaller rate of compounding in that cluster (Simultaneity is also smaller, but to a lesser extent). The relatively poor spatial match between the rain and wind regions in cluster 4 is the reason why it isn't the cluster associated with the highest rain-wind risk. Similarly, the reason why pm10-heat events have probabilities of occurrence closer to P_I than rain-wind and rain-wave events is that both simultaneity and overlap are higher. Very high values of Sim. and Over., around 80%, explain why cluster 6 exhibits the highest pm10-heat compound probabilities. This is due to the very high heat event probability associated with heat lows over the desert in that cluster, which means that most of the time a pm10 event occurs, a heat event is co-occurring. In general, clusters with higher compound event probabilities have higher single hazard Simultaneity and Overlap, with two interesting exceptions. First, simultaneity is fairly constant in Rain-Wave events, which

https://doi.org/10.5194/egusphere-2023-2322
Preprint. Discussion started: 17 October 2023

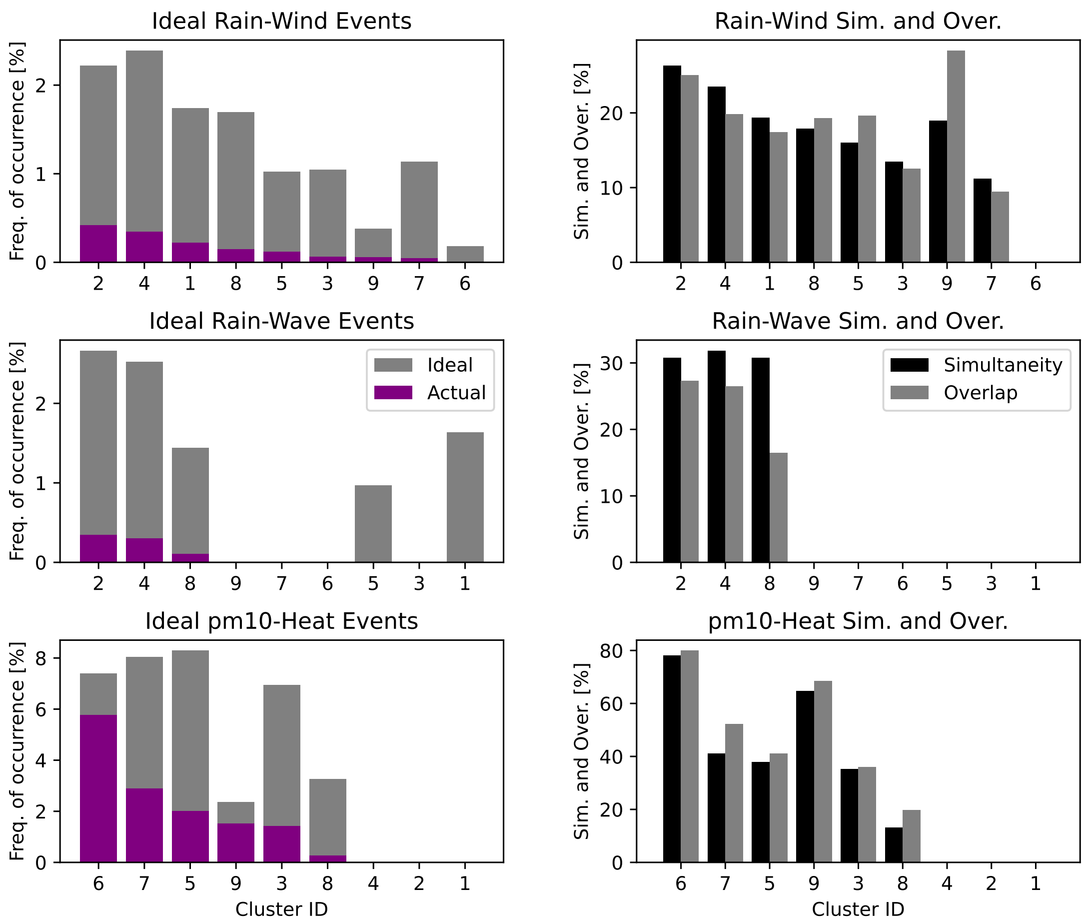

Figure 12. Left column: Ideal (grey bars) and Actual (purple bars) probabilities of occurrence of rain-wind (top), rain-wave (center) and pm10-heat (bottom) compound events. Right column: Simultaneity (black bars) and Overlap (grey bars) of individual hazards for rain-wind (top), rain-wave (center) and pm10-heat (bottom) compound events.

indicates that there are little variations across clusters of the distribution of individual hazard across cyclones within a cluster. Second, cluster 9, which is associated with cut-off lows (Givon et al., 2023) has high Overlap and simultaneity of events despite being associated with low probabilities of individual hazards.

https://doi.org/10.5194/egusphere-2023-2322
Preprint. Discussion started: 17 October 2023

4.2 Topography

Overlap is particularly small for rain-wind events. This is consistent with the very distinct rain and wind footprints in Fig.9, and may be due to the fact that cluster 2, 4 and 1 cyclones usually occur near the north shore of the Mediterranean, partly over water and partly over land. To illustrate the role of topography, Fig.9 shows the 300 m isohypse along with a contour for the 100 m per degree meridional slope. Note that storms from all these clusters occur just south of the 300 m altitude average line and of a high average gradient area. The isohypse corresponds well with contours of high wind event probability. This is likely due to the fact that, over rough topography, the 10 m s^{-1} lower wind threshold is higher than the 98th percentile of winds, and hence that wind events are, by our definition, less frequent in such areas. Precipitation tends to be more concentrated to the north of the cyclones, where it may be enhanced by the forced ascent over topography. Interestingly, topography is located closer to the average cyclone center in cluster 4, and extends further to the west. For that reason, wind events, and hence compound events are fewer to the northwest of the center, where they occur most frequently in cluster 2. Hence topography may cause a partition between rainy and windy areas in Mediterranean cyclones, and be responsible for the relatively small probability of rain-wind events in the region. Topography is not relevant to rain-wave compound events because only sea-level data points are considered, but it is worth noting that precipitation over the sea (Figs.5 and 10) has a similar magnitude as precipitation associated with all storms (Figs.4 and 9). This suggests that either topography does not enhance much the probability of rain events in Mediterranean cyclones, or that there is a compensating effect of moist air when storms occur over the sea.

4.3 Relation to dynamical features

We now turn to quantifying the relation between hazards and dynamical features such as warm conveyor belts, cold fronts and dry intrusions. To do so, we use the definitions introduced in section 2, and we compute the probability of co-occurrence of hazards with dynamical features. Figure 13 compares the probability of compound hazard with the joint probability of a compound hazard and a dynamical feature. First, note that the probabilities of co-occurrence with WCBs or with CFs are high and fairly similar for rain-wind and rain-wave events. This similarity of the magnitudes is certainly influenced by the definition of a 2.5 degrees region of influence around CF points introduced in section 2, but the good scaling between the CF and WCB probabilities is likely physical and due to the fact that both features tend to occur within the same cyclones. Then we see that dynamical features are associated with a far smaller fraction of pm10-heat events than of other compound events. This is likely because the cyclones associated with pm10-heat typically occur further south and in the summer, while the cyclones associated with rain, wind and waves are strongly baroclinic midlatitude winter cyclones. By contrast to their strong relation to WCBs and CFs, very few compound events co-occur with DIs. This result is partly due to the type of compound events considered; it makes sense that very few multivariate event involving precipitation would co-occur with dry intrusions. Other types of compound events not considered here, like waves and winds which poses a risk to navigation, would likely be more associated with dry intrusions. It also makes sense that DIs would not be very important in the weakly baroclinic cyclones of cluster 6, 7 and 5. Interestingly, the fraction of compound events where dynamical features are involved in rain-wind or rain-wave events is somewhat lower for the highest-risk cluster 2. This may be an indication that, in clusters associated with

https://doi.org/10.5194/egusphere-2023-2322
Preprint. Discussion started: 17 October 2023

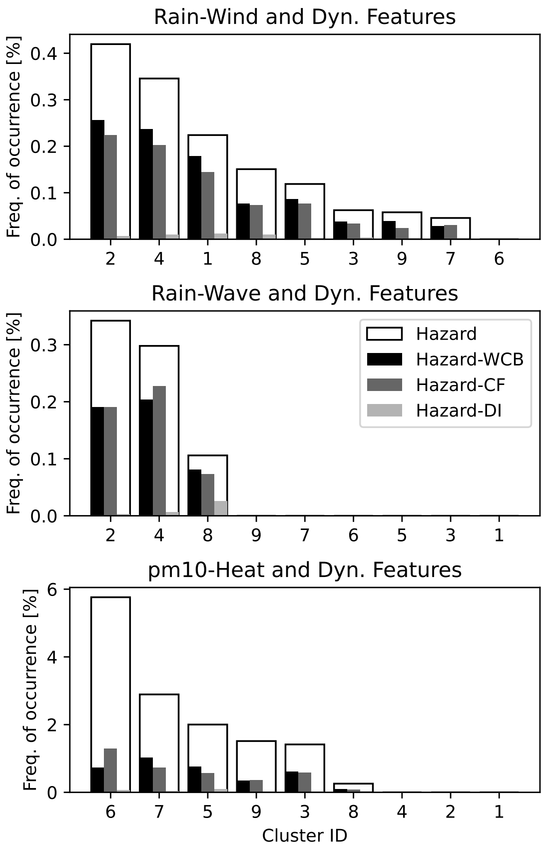

Figure 13. Probability of occurrence of rain-wind, rain-wave and pm10-heat compound hazards (broad white bars), and probability of co-occurrence of compound hazards with warm conveyor belts (WCB, black bars), cold fronts (CF, dark grey bars) and dry intrusions (DI, light grey bars). The clusters are sorted in descending order of hazard probability.

the most events, the surface cyclone itself is associated with enough rain, wind and waves events to cause a significant fraction of the compound events. In slightly weaker cyclones, like those of clusters 1 (rain-wind) or 8 (rain-wave), it may be that the presence of a well-defined front or conveyor belt is often necessary for compound events to occur.

To refine our understanding of the role of dynamical features, we now quantify their relation to individual hazards. Figure 14 compares the probabilities of individual hazards with the joint probabilities of individual hazards and of dynamical features. Here as in Fig. 13, the hazard-WCB joint probabilities scale fairly well with the hazard-CF joint probabilities for all clusters

https://doi.org/10.5194/egusphere-2023-2322
Preprint. Discussion started: 17 October 2023

and for a given hazard. From hazard to hazard, however, the relative magnitudes of WCB and CF co-occurrence probabilities vary substantially. For example, the joint probabilities of rain events with WCBs are always larger than with CFs, while on the contrary, the joint probabilities of wind or wave events with WCBs are always smaller than with CFs. We interpret these results to mean that, while CFs and WCBs tend to occur within the same cyclones, WCBs are more important in controlling precipitation in Mediterranean cyclones, while CFs are more important for wind and wave events. As a result, for the compound events considered in Fig.13, which require the joint occurrence of both rain and wind, or rain and wave events, the relative roles of WCBs and CFs are more balanced.

Almost no rain events are associated with dry intrusions, which explains the lack of association of that feature with compound events involving rain. Dry intrusions have small but non-zero joint probabilities with wind, waves or pm10, and wave events are the only ones where DIs become more important than other dynamical features (clusters 8 and 5). DIs tend to occur far from the storm centers, in storm-relative regions where the hazards are more diffuse and rarely statistically significant. The fact that we are only accounting for hazards in statistically significant areas here may explain the relatively small role of dry intrusions with respect to other dynamical features. It is likely that accounting directly for the relation between features and hazards without taking storm relative composites would reveal a larger role for dry intrusions, but such an analysis exceeds the scope of this climatology. Overall, dynamical features play the largest role in rain events, where they are associated with more than half of all events, a smaller role in wind and wave events, where they are associated with a third to half of the events, and an even smaller role in pm10 events. Note that the cluster associated with the highest probability of pm10 events is cluster 4, for which WCBs, CFs and DIs all play a role, albeit not very large. While it isn't associated with any significant probability of pm10-heat events, given the relatively high latitude at which cyclones occur in that cluster (see Fig.7), and its strong association with pm10 events, it is likely that the Type B frontal cyclones of cluster 4 are major contributors in transporting dust from the Sahara to Europe.

5 Conclusions

Mediterranean cyclones, despite their relatively small sizes and intensities, are associated with much of the weather-induced damage in the region (Flaounas et al., 2015, 2022). While our fundamental understanding of Mediterranean cyclones, has progress rapidly, our understanding of the associated hazards and impacts remains somewhat limited, owing to the complexity of the Mediterranean basin and the recency of extensive research on the topic (Flaounas et al., 2022). For example, while the relation between many individual hazards and Mediterranean cyclones is already fairly well understood, the relation between Mediterranean cyclones and the potentially more impactful multivariate hazards (Zscheischler et al., 2018) remains to be characterized. To fill this knowledge gap, we aimed to establish a climatology of the compound hazards that occur in association with Mediterranean cyclones. To that effect, we devised a simple method to compute storm-relative composites of multivariate compound events, and evaluate their statistical significance. Composites were computed for rain-wind, rain-wave (which required evaluating land-masked composites) and pm10-heat events. These three types of multivariate events were selected

https://doi.org/10.5194/egusphere-2023-2322
Preprint. Discussion started: 17 October 2023

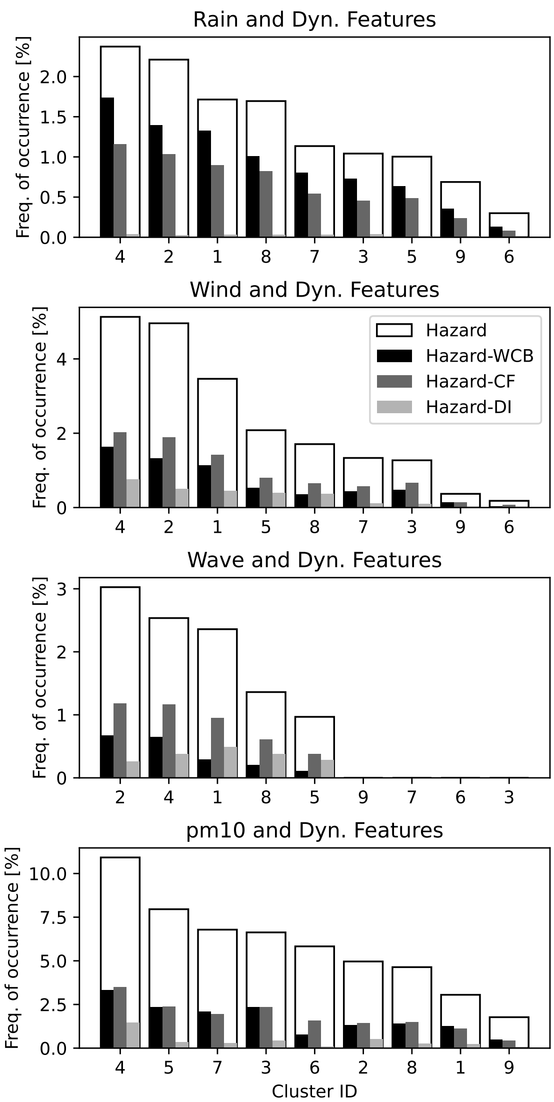

Figure 14. Probability of occurrence of rain, wind, wave and pm10 individual hazards (broad white bars), and probability of co-occurrence of individual hazards with warm conveyor belts (WCB, black bars), cold fronts (CF, dark grey bars) and dry intrusions (DI, light grey bars). The clusters are sorted in descending order of hazard probability.

https://doi.org/10.5194/egusphere-2023-2322
Preprint. Discussion started: 17 October 2023

because they consider multiple individual hazards and a broad range of societal impacts, from infrastructure damage to human health. To help assess the role of the large-scale environment, the climatology is based on a state-of-the-art cyclone tracks dataset for the region (Flaounas et al., 2023) and a classification of those tracks based on the upper-level PV field associated with the cyclones (Givon et al., 2023). In addition, to assess the role of dynamical features, we evaluated the probabilities of co-occurrence of the compound events and of warm conveyor belts, cold fronts and dry intrusions.

We showed that distinct large-scale contexts are associated with different types of compound events in Mediterranean cyclones. Namely, rain-wind and rain-wave events are mostly due to type A and B cyclones as well as Rossby wave breaking near the Mediterranean north shore in cold seasons, while pm10-heat events are due to heat lows, daughter cyclones and anticyclonic wave breaking in North-Africa, predominantly during warm seasons. Event probability footprints varies between storm clusters but much more so between hazards. In general, wind events are concentrated to the south of the storms, rain events are concentrated to the north, wave events are concentrated to the west, and dust events are concentrated either around the storm center or to the south. The compound hazard footprint shapes then depend upon the relative positions of the individual hazard footprints, with rain-wind event probabilities peaking west-north-west of the cyclone centers, rain-wave events peaking to the north, and pm10-heat events being distributed around the storm centers. We find that the probabilities of compound events depend mainly on the probabilities of individual hazards, but also on how well these hazards coincide temporally and spatially. To understand how high compounding probabilities arise, we introduce the Simultaneity and Overlap parameters which reveal that in general, individual hazards coincide at a higher rate in clusters associated with high compounding probabilities. For example, the anticylonic wave breaking cyclones of cluster 2 are associated with the most rain-wind events because the individual hazard footprints overlap particularly well. Finally, we quantified the relation between dynamical features and compound events, and we found that warm conveyor belts and cold fronts where both equally important for rain-wind and rain-wave events, while no dynamical feature was critical to the occurrence of pm10-heat events. Dynamical features where shown to co-occur more frequently with compound events in clusters associated with a smaller probability of compound events.

We hope that the information provided here will help interpret the risk posed by different weather systems in the Mediterranean, and infer how that risk may change in the future. For example, the observation that the frequency of cluster 6 heat lows has been increasing in recent decades (Givon et al., 2023) suggests that an increase in pm10 and heat events is probably currently occurring and may be expected to continue. Next steps in the present research endeavour will include establishing an Eulerian climatology of compound events in association with cyclones in the Mediterranean region.

Code availability. The code used to produce analyses is available upon request.

https://doi.org/10.5194/egusphere-2023-2322
Preprint. Discussion started: 17 October 2023

Author contributions. Raphaël Rousseau-Rizzi, Olivia Martius, Shira Raveh-Rubin and and Jennifer Catto designed the study. Raphaël Rousseau-Rizzi developed the analysis code and performed the analyses. Raphaël Rousseau-Rizzi prepared the manuscript with contributions from all co-authors.

Competing interests. At least one of the (co-)authors is a member of the editorial board of Weather and Climate Dynamics.

Acknowledgements. The authors would like to thank the Swiss National Science foundation for supporting this work under grant number IZCOZ0 205461. The authors would also like to thank the MedCyclones COST action for facilitating meetings on the topic of this study, and the participants to the meetings, for stimulating discussions and insight. Finally, the authors would like to thank Katharina Heitmann and Michael Sprenger for providing the warm conveyor belt data used in this study.

References

Amores, A., Marcos, M., Carrió, D. S., and Gómez-Pujol, L.: Coastal impacts of Storm Gloria (January 2020) over the north-western Mediterranean, Natural Hazards and Earth System Sciences, 20, 1955–1968, https://doi.org/10.5194/nhess-20-1955-2020, 2020.

Aragão, L. and Porcù, F.: Cyclonic activity in the Mediterranean region from a high-resolution perspective using ECMWF ERA5 dataset, Climate Dynamics, 58, 1293–1310, https://doi.org/10.1007/s00382-021-05963-x, 2022.

Barbariol, F., Davison, S., Falcieri, F. M., Ferretti, R., Ricchi, A., Sclavo, M., and Benetazzo, A.: Wind Waves in the Mediterranean Sea: An ERA5 Reanalysis Wind-Based Climatology, Frontiers in Marine Science, https://doi.org/10.3389/fmars.2021.760614, 2021.

Bevacqua, E., Maraun, D., Vousdoukas, M., Voukouvalas, E., Vrac, M., Mentaschi, L., and Widmann, M.: Higher probability of compound flooding from precipitation and storm surge in Europe under anthropogenic climate change, Science advances, 5, eaaw5531, https://doi.org/10.1126/sciadv.aaw5531, 2019.

Bou Karam, D., Flamant, C., Cuesta, J., Pelon, J., and Williams, E.: Dust emission and transport associated with a Saharan depression: February 2007 case, Journal of Geophysical Research: Atmospheres, 115, https://doi.org/10.1029/2009JD012390, 2010.

Catto, J. L. and Dowdy, A.: Understanding compound hazards from a weather system perspective, Weather and Climate Extremes, 32, 100 313, https://doi.org/10.1016/j.wace.2021.100313, 2021.

Catto, J. L. and Pfahl, S.: The importance of fronts for extreme precipitation, Journal of Geophysical Research: Atmospheres, 118, 10–791, https://doi.org/10.1002/jgrd.50852, 2013.

Cavaleri, L., Bertotti, L., Torrisi, L., Bitner-Gregersen, E., Serio, M., and Onorato, M.: Rogue waves in crossing seas: The Louis Majesty accident, Journal of Geophysical Research: Oceans, 117, https://doi.org/10.1029/2012JC007923, 2012.

Dayan, U., Ziv, B., Shoob, T., and Enzel, Y.: Suspended dust over southeastern Mediterranean and its relation to atmospheric circulations, International Journal of Climatology: A Journal of the Royal Meteorological Society, 28, 915–924, https://doi.org/10.1002/joc.1587, 2008.

Dowdy, A. J. and Catto, J. L.: Extreme weather caused by concurrent cyclone, front and thunderstorm occurrences, Scientific reports, 7, 1–8, https://doi.org/10.1038/srep40359, 2017.

Emanuel, K.: Genesis and maintenance of "Mediterranean hurricanes", Advances in Geosciences, 2, 217–220, https://doi.org/10.5194/adgeo-2-217-2005, 2005.

EU and Parliament, E.: Directive 2008/50/EC of the European Parliament and of the Council of 21 May 2008 on ambient air quality and cleaner air for Europe, Official Journal of the European Union, 2008.

Flaounas, E., Raveh-Rubin, S., Wernli, H., Drobinski, P., and Bastin, S.: The dynamical structure of intense Mediterranean cyclones, Climate Dynamics, 44, 2411–2427, https://doi.org/10.1007/s00382-014-2330-2, 2015.

Flaounas, E., Kotroni, V., Lagouvardos, K., Gray, S. L., Rysman, J.-F., and Claud, C.: Heavy rainfall in Mediterranean cyclones. Part I: contribution of deep convection and warm conveyor belt, Climate dynamics, 50, 2935–2949, https://doi.org/10.1007/s00382-017-3783-x, 2018.

Flaounas, E., Davolio, S., Raveh-Rubin, S., Pantillon, F., Miglietta, M. M., Gaertner, M. A., Hatzaki, M., Homar, V., Khodayar, S., Korres, G., et al.: Mediterranean cyclones: Current knowledge and open questions on dynamics, prediction, climatology and impacts, Weather and Climate Dynamics, 3, 173–208, https://doi.org/10.5194/wcd-3-173-2022, 2022.

Flaounas, E., Aragão, L., Bernini, L., Dafis, S., Doiteau, B., Flocas, H., L. Gray, S., Karwat, A., Kouroutzoglou, J., Lionello, P., et al.: A composite approach to produce reference datasets for extratropical cyclone tracks: application to Mediterranean cyclones, Weather and Climate Dynamics Discussions, 2023, 1–32, https://doi.org/10.5194/wcd-4-639-2023, 2023.

https://doi.org/10.5194/egusphere-2023-2322
Preprint. Discussion started: 17 October 2023

Flocas, H.: Diagnostics of cyclogenesis over the Aegean Sea using potential vorticity inversion, Meteorology and Atmospheric Physics, 73, 25–33, https://doi.org/10.1007/s007030050061, 2000.

Givon, Y., Hess, O., Flaounas, E., Catto, J. L., Sprenger, M., and Raveh-Rubin, S.: Process-based classification of Mediterranean cyclones using potential vorticity, EGUsphere, 2023, 1–36, https://doi.org/10.5194/egusphere-2023-1247, 2023.

Heitmann, K., Sprenger, M., Binder, H., Wernli, H., and Joos, H.: Warm conveyor belt characteristics and impacts along the life cycle of extratropical cyclones: Case studies and climatological analysis based on ERA5, EGUsphere, 2023, 1–42, https://doi.org/10.5194/egusphere-2023-1092, 2023.

Hennermann, K. and Berrisford, P.: ERA5: Data description, Copernicus knowledge base, 2020.

Hersbach, H., Bell, B., Berrisford, P., Hirahara, S., Horányi, A., Muñoz-Sabater, J., Nicolas, J., Peubey, C., Radu, R., Schepers, D., et al.: The ERA5 global reanalysis, Quarterly Journal of the Royal Meteorological Society, 146, 1999–2049, https://doi.org/10.1002/qj.3803, 2020.

Inness, A., Ades, M., Agustí-Panareda, A., Barré, J., Benedictow, A., Blechschmidt, A.-M., Dominguez, J. J., Engelen, R., Eskes, H., Flemming, J., et al.: The CAMS reanalysis of atmospheric composition, Atmospheric Chemistry and Physics, 19, 3515–3556, https://doi.org/10.5194/acp-19-3515-2019, 2019.

Kalkstein, A. J., Rudich, Y., Raveh-Rubin, S., Kloog, I., and Novack, V.: A closer look at the role of the cyprus low on dust events in the Negev Desert, Atmosphere, 11, 1020, https://doi.org/10.3390/atmos11101020, 2020.

Katsouyanni, K., Pantazopoulou, A., Touloumi, G., Tselepidaki, I., Moustris, K., Asimakopoulos, D., Poulopoulou, G., and Trichopoulos, D.: Evidence for interaction between air pollution and high temperature in the causation of excess mortality, Archives of Environmental Health: An International Journal, 48, 235–242, https://doi.org/10.1080/00039896.1993.9940365, 1993.

Klawa, M. and Ulbrich, U.: A model for the estimation of storm losses and the identification of severe winter storms in Germany, Natural Hazards and Earth System Sciences, 3, 725–732, https://doi.org/10.5194/nhess-3-725-2003, 2003.

Kohonen, T.: The self-organizing map, Proceedings of the IEEE, 78, 1464–1480, https://doi.org/10.1109/5.58325, 1990.

Martius, O., Pfahl, S., and Chevalier, C.: A global quantification of compound precipitation and wind extremes, Geophysical Research Letters, 43, 7709–7717, https://doi.org/10.1002/2016GL070017, 2016.

Miglietta, M. M.: Mediterranean tropical-like cyclones (Medicanes), Atmosphere, 10, 206, https://doi.org/10.3390/atmos10040206, 2019.

Nissen, K. M., Leckebusch, G. C., Pinto, J. G., and Ulbrich, U.: Mediterranean cyclones and windstorms in a changing climate, Regional environmental change, 14, 1873–1890, https://doi.org/10.1007/s10113-012-0400-8, 2014.

Patlakas, P., Stathopoulos, C., Tsalis, C., and Kallos, G.: Wind and wave extremes associated with tropical-like cyclones in the Mediterranean basin, International Journal of Climatology, 41, E1623–E1644, https://doi.org/10.1002/joc.6795, 2021.

Petterssen, S. and Smebye, S.: On the development of extratropical cyclones, Quarterly Journal of the Royal Meteorological Society, 97, 457–482, https://doi.org/10.1002/qj.49709741407, 1971.

Pfahl, S. and Wernli, H.: Quantifying the relevance of cyclones for precipitation extremes, Journal of Climate, 25, 6770–6780, https://doi.org/10.1175/JCLI-D-11-00705.1, 2012.

Raveh-Rubin, S.: Dry intrusions: Lagrangian climatology and dynamical impact on the planetary boundary layer, Journal of Climate, 30, 6661–6682, https://doi.org/10.1175/JCLI-D-16-0782.1, 2017.

Raveh-Rubin, S. and Wernli, H.: Large-scale wind and precipitation extremes in the Mediterranean: a climatological analysis for 1979–2012, Quarterly Journal of the Royal Meteorological Society, 141, 2404–2417, https://doi.org/10.1002/qj.2531, 2015.

Rémy, S., Kipling, Z., Flemming, J., Boucher, O., Nabat, P., Michou, M., Bozzo, A., Ades, M., Huijnen, V., Benedetti, A., et al.: Description and evaluation of the tropospheric aerosol scheme in the European Centre for Medium-Range Weather Forecasts (ECMWF) Integrated

https://doi.org/10.5194/egusphere-2023-2322
Preprint. Discussion started: 17 October 2023

Forecasting System (IFS-AER, cycle 45R1), Geoscientific Model Development, 12, 4627–4659, https://doi.org/10.5194/gmd-15-4881-2022, 2019.

Rivoire, P., Martius, O., and Naveau, P.: A comparison of moderate and extreme ERA-5 daily precipitation with two observational data sets, Earth and Space Science, 8, e2020EA001 633, https://doi.org/10.1029/2020EA001633, 2021.

Saleh, F., Ramaswamy, V., Wang, Y., Georgas, N., Blumberg, A., and Pullen, J.: A multi-scale ensemble-based framework for forecasting compound coastal-riverine flooding: The Hackensack-Passaic watershed and Newark Bay, Advances in Water Resources, 110, 371–386, https://doi.org/10.1016/j.advwatres.2017.10.026, 2017.

Thorncroft, C., Hoskins, B., and McIntyre, M.: Two paradigms of baroclinic-wave life-cycle behaviour, Quarterly Journal of the Royal Meteorological Society, 119, 17–55, https://doi.org/10.1002/qj.49711950903, 1993.

Ulbrich, U., Leckebusch, G. C., and Pinto, J. G.: Extra-tropical cyclones in the present and future climate: a review, Theoretical and Applied Climatology, 96, 117–131, https://doi.org/10.1007/s00704-008-0083-8, 2009.

Welker, C., Martius, O., Froidevaux, P., Reijmer, C. H., and Fischer, H.: A climatological analysis of high-precipitation events in Dronning Maud Land, Antarctica, and associated large-scale atmospheric conditions, Journal of Geophysical Research: Atmospheres, 119, 11–932, https://doi.org/10.1002/2014JD022259, 2014.

WHO and for Environment, E. C.: WHO global air quality guidelines: particulate matter (PM2. 5 and PM10), ozone, nitrogen dioxide, sulfur dioxide and carbon monoxide, World Health Organization, 2021.

Wilks, D.: "The stippling shows statistically significant grid points": How research results are routinely overstated and overinterpreted, and what to do about it, Bulletin of the American Meteorological Society, 97, 2263–2273, https://doi.org/10.1175/BAMS-D-15-00267.1, 2016.

Zscheischler, J., Westra, S., Van Den Hurk, B. J., Seneviratne, S. I., Ward, P. J., Pitman, A., AghaKouchak, A., Bresch, D. N., Leonard, M., Wahl, T., et al.: Future climate risk from compound events, Nature Climate Change, 8, 469–477, https://doi.org/10.1038/s41558-018-0156-3, 2018.

Zscheischler, J., Martius, O., Westra, S., Bevacqua, E., Raymond, C., Horton, R. M., van den Hurk, B., AghaKouchak, A., Jézéquel, A., Mahecha, M. D., et al.: A typology of compound weather and climate events, Nature reviews earth & environment, 1, 333–347, https://doi.org/10.1038/s43017-020-0060-z, 2020.